PHYSICAL REVIEW B **88**, 155101 (2013)

Infrared anomalous Hall effect in $Ca_xSr_{1-x}RuO_3$ films

M.-H. Kim,[1,2] T. Tanaka,[3] C. T. Ellis,[1] A. Mukherjee,[1] G. Acbas,[1] I. Ohkubo,[4] H. Christen,[5]
D. Mandrus,[5] H. Kontani,[3] and J. Cerne[1]

[1]*Department of Physics, University at Buffalo, The State University of New York, Buffalo, New York 14260, USA*
[2]*Department of Physics, University of Maryland, College Park, Maryland 20742, USA*
[3]*Department of Physics, Nagoya University, Furo-cho, Nagoya 464-8602, Japan*
[4]*Department of Applied Chemistry, University of Tokyo, Tokyo, Japan*
[5]*Oak Ridge National Laboratory, Condensed Matter Science Division, Oak Ridge, Tennessee 37831, USA*

(Received 2 May 2013; published 1 October 2013)

The midinfrared anomalous Hall effect (AHE) can provide critical new information for resolving the controversial origins of the dc AHE in $Ca_xSr_{1-x}RuO_3$. The complex Faraday and Kerr angles, as well as the complex Hall conductivity σ_{xy}, are measured in $Ca_xSr_{1-x}RuO_3$ films as a function of mid- and near-infrared energy E from 0.1 eV to 1.4 eV, magnetic field H, temperature T, and Ca concentration x. For the ferromagnetic state from $x = 0$ to 0.4, the (d_{xz}, d_{yz})-orbital tight-binding model is employed to investigate the quasiparticle role in the low energy response of the AHE $\sigma_{xy}(E)$ since the Berry curvature term becomes weak at low energies. The infrared Hall sign reversals with T are observed only at $x = 0$ and 0.13, which is narrower than the Ca concentration range in which the dc Hall sign reversal appears. The similarity of the infrared Hall angles between paramagnetic and ferromagnetic $Ca_xSr_{1-x}RuO_3$ compounds demonstrates the symmetric nature of the Hall response around the quantum phase transition at $x = 0.7$.

DOI: 10.1103/PhysRevB.88.155101 PACS number(s): 78.20.Ls, 78.66.Bz, 75.50.Cc, 75.47.Lx

I. INTRODUCTION

The anomalous Hall effect (AHE) is found in a wide range of interesting materials and its origins are rich and controversial. The AHE appears typically in metallic ferromagnets as a result of spin-orbit coupling.[1] There have been numerous studies on intrinsic Berry-phase contribution to the AHE in metallic ferromagnets, but it is difficult to separate it from the quasiparticle contribution to the AHE at dc experimentally. To distinguish these contributions to the AHE, higher probing energies can be used to tune the quasiparticle scattering rate, which is quite strong up to midinfrared energies in the metallic ferromagnet. This tunability is critical to resolving the role of quasiparticles in the AHE. Hall conductivity data of the metallic ferromagnet $SrRuO_3$ at mid- and near-infrared energies (MNIR) agree remarkably well with predictions from an intrinsic Berry-phase model.[2] However, the intrinsic and extrinsic mechanisms still have not been resolved at dc and low energies near dc.[3,4] For this reason, $Ca_xSr_{1-x}RuO_3$ compounds have been a good candidate for studying the origins of the AHE in $SrRuO_3$ since the ferromagnetism in $Ca_xSr_{1-x}RuO_3$ compounds can be gradually weakened by adding Ca atoms, allowing a more controlled exploration of the AHE.[5] Moreover, the dc Hall response changes at the quantum phase transition (QPT) from ferromagnetic ($x \leqslant 0.7$) to paramagnetic ($x \geqslant 0.75$). The two end materials $SrRuO_3$ and $CaRuO_3$ show a dc Hall sign reversal with the temperature but they may have different origins.[6] In fact, the temperature dependence of the dc Hall angle in paramagnetic $CaRuO_3$ looks more like that in ferromagnetic $SrRuO_3$ than the nearby higher Ca concentration $Ca_xSr_{1-x}RuO_3$ paramagnetic samples. So far, there have been extensive dc Hall measurements in $Ca_xSr_{1-x}RuO_3$ compounds,[5,7,8] but no infrared Hall studies in these materials except $x = 0$.[2,4]

In recent work, we have compared MNIR (115–1400 meV) Hall measurements in $SrRuO_3$ with predictions from the Berry phase calculations.[4] The Berry phase calculation of the intrinsic AHE by Fang and co-workers[2,7,8] can explain the anomalous Hall sign reversal with temperature in $SrRuO_3$ at dc and accurately predicts the ac Hall conductivity $\sigma_{xy}^{\mathrm{AHE}}(E)$ above $E = 200$ meV.[4] However, the disagreement between the intrinsic Berry phase calculation and the measured longitudinal conductivity $\sigma_{xx}(E)$ below 200 meV clearly shows that the excitations of quasiparticles (intraband transitions) are important at lower energies. Because θ_H at 100 meV and at dc have similar magnitudes, similar temperature dependence, and change sign at a similar temperature, θ_H at 100 meV appears to originate from the same mechanism as the dc θ_H. Since both Berry phase and extrinsic scattering mechanisms can explain the dc Hall sign reversal with temperature,[2,3] we cannot completely rule out the intrinsic Berry phase contribution to AHE near dc. However, we expect quasiparticles to play an important role in the AHE at low frequencies.

The quasiparticle contribution to AHE can be either extrinsic (scattering) or intrinsic. The extrinsic contribution of quasiparticles to AHE has been studied extensively at dc. The extrinsic AHE arises from impurity scattering and the intrinsic AHE is due to the band structure.[1] The extrinsic AHE has been reported mostly at dc where impurity scattering is dominant. For this mechanism, the Hall sign reversal is due to a competition between skew scattering[9–11] and side-jump scattering.[12–15] Although one expects the extrinsic ac anomalous Hall effect to vanish at high frequencies, where ac-driven carriers undergo many oscillations between scattering events, no quantitative theoretical predictions have been made to explore how the extrinsic AHE evolves at finite frequencies. The intrinsic contribution of quasiparticles in transition metal ferromagnets has been studied theoretically by Kontani *et al.* using a (d_{xz}, d_{yz})-orbital tight-binding model.[16] The anomalous velocity originates from the quasiparticle hopping integral between two neighboring d orbitals. Kontani *et al.* calculated all possible intrinsic AHE contributions including a Berry curvature term and a quasiparticle term (Fermi surface term) at dc and finite frequencies. The model claims that the quasiparticle damping rate γ is an important parameter at lower energies. Since the Berry curvature term is insensitive to γ, the Berry curvature calculation agrees well at higher frequencies but the agreement worsens in the lower frequency regime. They found that the intrinsic quasiparticle term is important for reliably reproducing measured data for finite γ at low frequencies, whereas the Berry curvature term almost cancels with the other contributions to the anomalous Hall conductivity at dc.

In this paper, we extended our infrared AHE study on SrRuO$_3$ to Ca$_x$Sr$_{1-x}$RuO$_3$ compounds using the MNIR Faraday (θ_F) and Kerr (θ_K) angle measurements. Adding Ca decreases the Curie temperature (T_c) and leads to a quantum critical phase transition at $x \approx 0.7$ as the material goes from ferromagnetic to paramagnetic. As in Ref. 4, we have made a systematic study of the temperature, magnetic field, and frequency dependence of the Hall response of Ca$_x$Sr$_{1-x}$RuO$_3$ in the energy range from 0.1 eV to 1.4 eV. This range shows strong spectral features for σ_{xy} in SrRuO$_3$ and we expect similar spectral features and systematic changes with Ca concentration for σ_{xy} in Ca$_x$Sr$_{1-x}$RuO$_3$ compounds. Additionally, we expect the Hall response to be symmetric around the quantum phase transition at $x \approx 0.7$.

II. EXPERIMENTAL SYSTEM

Our previous work in SrRuO$_3$ demonstrates that MNIR magnetopolarimetry measurements are a good tool to study unusual Hall properties, which often exhibit strong spectral features in MNIR.[4,17] MNIR Hall measurements have been applied to various systems such as cuprate high temperature superconductors,[18–20] diluted magnetic semiconductors,[13,17,21] and ruthenate perovskite materials[2] to obtain the intrinsic electronic structure and the energy scales of the system.[22]

The Faraday and Kerr angles from Ca$_x$Sr$_{1-x}$RuO$_3$ samples are measured using a sensitive polarization modulation technique[23–25] in MNIR spectral range (115–1400 meV). The Ca$_x$Sr$_{1-x}$RuO$_3$ samples are grown by pulsed laser deposition at Oak Ridge National Laboratory as described in Refs. 26 and 27. Various gas lasers, semiconductor lasers, and a custom-modified double pass prism monochromator with a Xe light source allow us to perform measurements over a wide probe energy range. For details of the experimental technique, see Refs. 24 and 25. The complex θ_F and θ_K angles are measured in the MNIR spectral range as a function of magnetic field up to 2 T and temperature from 10 K to 300 K. The small background Faraday and Kerr signals from the cryostat windows and the film substrate have been subtracted from the data. The complex conductivities σ_{xx} and σ_{xy} are determined directly from the measured complex θ_F and θ_K using analysis techniques in Ref. 24.

III. FERROMAGNETIC REGION ($x \leqslant 0.7$)

The ferromagnetic transition (Curie) temperature T_c of SrRuO$_3$ is suppressed by the substitution of Sr atoms with Ca atoms. Magnetization and magnetoresistance ρ_{xx} measurements at dc demonstrate that T_c decreases linearly as Ca composition increases up to $x = 0.7$.[26] Unlike ρ_{xx}, the magnetic field H dependence of the dc Hall resistivity $\rho_{xy}(H)$ at temperature $T = 5$ K changes dramatically in sign and magnitude at low Ca composition near $x = 0.2$.[5] We expect the AHE Faraday and Kerr angles in Ca$_x$Sr$_{1-x}$RuO$_3$ to behave similarly to ρ_{xy} since θ_F and θ_K are proportional to ρ_{xy}.[24] We first explore the AHE θ_F and θ_K in a Ca composition $x \leqslant 0.47$ where the signals are large and their hysteretic behavior allows us to separate the AHE from the ordinary Hall effect (OHE). Figure 1 shows the energy dependence of AHE θ_F and θ_K for Ca composition $x = 0$ to 0.47 at $T = 10$ K and $H = 0$ T with the sample fully magnetized out of plane. The Hall signal at $H = 0$ T is purely anomalous because the OHE signal is proportional to H, while the AHE is proportional to the magnetization M. In addition, the OHE contribution is weaker as probing energy (E) increases.[4] Both the AHE θ_F and θ_K display strong probing energy and Ca composition dependence. The dc values of Re(θ_F) in Fig. 1(a) and Re(θ_K) in Fig. 1(c) are determined in Ref. 5, and connect smoothly with the infrared values as energy approaches zero. As the Ca composition increases, both AHE θ_F and θ_K become flatter and are less sensitive to energy. A small amount of Ca makes a significant change in the AHE θ_F at low energies of 0.1–0.3 eV compared to other energies where the basic shapes of θ_F and θ_K are maintained and only the overall magnitudes change systematically. This suggests that low energy AHE features are much more sensitive to the Ca composition than high energy features. The most prominent features at lower energy are in the AHE Re(θ_F) and Im(θ_F) at 0.1 eV as shown in Figs. 1(a) and 1(b). Both Re(θ_F) and Im(θ_F) at 0.1 eV cross zero near $x = 0.2$. These are consistent with dc $\rho_{xy}(H)$ hysteresis loops, which invert near $x = 0.2$.[5] The Re(θ_F) near 0.3 eV remains relatively constant over the $x = 0$–0.47 Ca composition range. For Im(θ_F), the dip near 0.2 eV slightly shifts to higher energy and decreases in magnitude as the Ca composition increases.

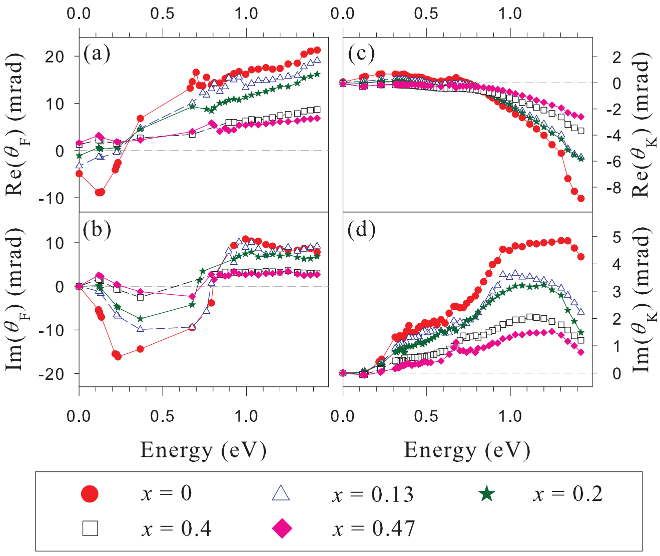

FIG. 1. (Color online) Energy dependence of the infrared AHE θ_F and θ_K for the Ca composition $x = 0$ to 0.47. The AHE (a) Re(θ_F), (b) Im(θ_F), (c) Re(θ_K), and (d) Im(θ_K) with the sample fully magnetized perpendicular to the sample surface at 0 T and 10 K. The intensity of transmitted light is too weak to measure θ_F in the 0.4–0.7 eV energy range.

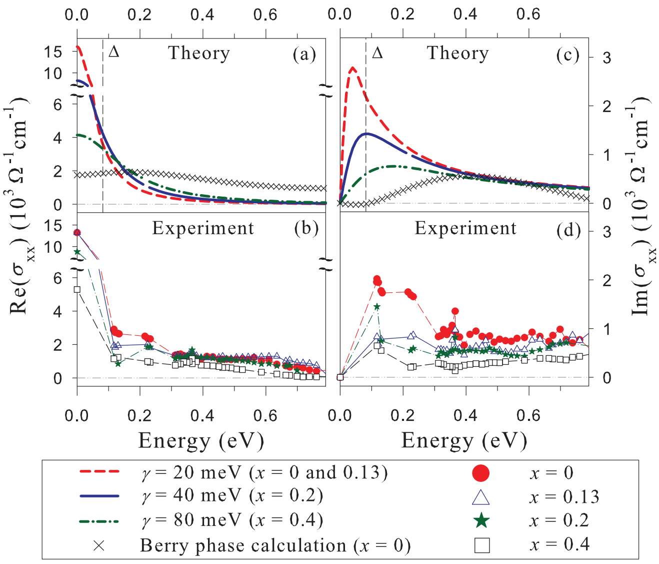

FIG. 2. (Color online) Infrared longitudinal conductivity σ_{xx} for the Ca composition $x = 0$ to 0.4. (a) Calculated and (b) measured Re(σ_{xx}), and (c) calculated and (d) measured Im(σ_{xx}). Lines in (a) and (c) present the (d_{xz}, d_{yz})-orbital tight binding model calculation. γ is the quasiparticle damping rate. The vertical dashed lines in (a) and (c) indicate the minimum band splitting energy $\Delta = 82$ meV. Symbols (×) in (a) and (c) shows the Berry phase calculation of the intrinsic AHE in SrRuO_3 by Fang *et al.*[2] σ_{xx} in (b) and (d) were obtained from AHE θ_F and θ_K in Fig. 1 by using the analysis technique in Ref. 24. All measurements were performed at $T = 10$ K. Note that the error bar is about 10–15% of the data.

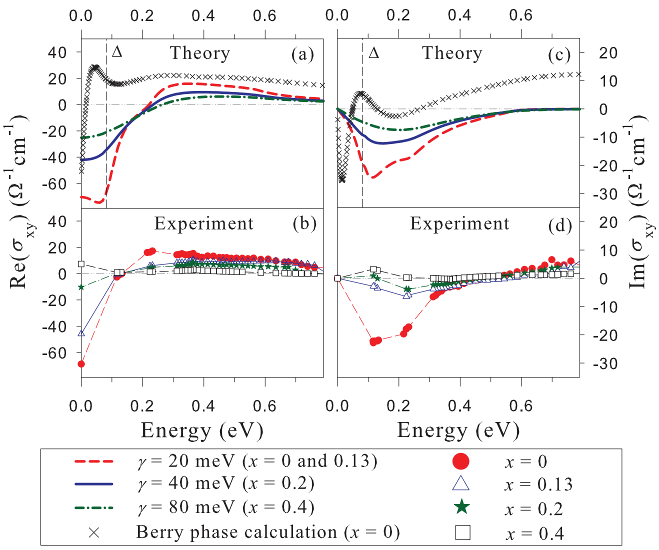

FIG. 3. (Color online) Transverse AHE conductivity σ_{xy} for the Ca composition $x = 0$ to 0.4. (a) Calculated and (b) measured Re(σ_{xy}), and (c) calculated and (d) measured Im(σ_{xy}). Lines in (a) and (c) present the (d_{xz}, d_{yz})-orbital tight binding model calculation. γ is the quasiparticle damping rate. Vertical dashed lines in (a) and (c) indicate minimum band splitting $\Delta = 82$ meV. Symbols (×) in (a) and (c) shows the Berry phase calculation of the intrinsic AHE in SrRuO_3 by Fang *et al.*[2] σ_{xy} in (b) and (d) were obtained from AHE θ_F and θ_K in Fig. 1 by using the analysis technique in Ref. 24. All measurements were performed at $T = 10$ K. Note that the error bar is about 2.5% of the data.

Two theoretical approaches, the Berry phase calculation and (d_{xz},d_{yz})-orbital tight-binding calculation, are employed here to examine the measured $\sigma_{xx}(E)$ and AHE $\sigma_{xy}(E)$ of $\mathrm{Ca}_x\mathrm{Sr}_{1-x}\mathrm{RuO}_3$. Figures 2 and 3 show the calculated and the measured complex $\sigma_{xx}(E)$ and AHE $\sigma_{xy}(E)$ for Ca composition from $x = 0$ to 0.4, although major differences between the two models are clearest in the frequency range from dc to two or three times of Δ, where we see differences over the entire measurement range. Due to a weak quasiparticle contribution in the Berry phase model, σ_{xx} shows completely different features in the two models over a wide frequency range. For example, in Fig. 2(a), Re(σ_{xx}) from the Berry phase model is relatively flat while the tight-binding model and measurements show a strong decrease in Re(σ_{xx}) from its dc value as energy increases. A further clear difference between the two models is shown in Fig. 2(c). While Im(σ_{xy}) from the Berry phase model is close to zero from dc to Δ, the tight-binding model predicts a sharp peak near Δ, which is consistent with the measured spectrum shown in Fig. 2(d). The disagreement between the Berry phase calculation and the measured values of $\sigma_{xx}(E)$ in $\mathrm{Ca}_x\mathrm{Sr}_{1-x}\mathrm{RuO}_3$ in Fig. 2 indicates that the quasiparticle contribution is more important at lower energies. A key difference between the two models can be seen in Re(σ_{xy}) in Fig. 3(a). Both the tight-binding model and the measurement show a zero crossing in Re(σ_{xy}) near Δ, well away from dc. Furthermore, Im(σ_{xy}) from the tight-binding model and the measurement in Fig. 3(c) and Fig. 3(d) show good quantitative and qualitative agreement and differ strongly from the small peak and dip in Im(σ_{xy}) near zero frequency predicted by the Berry phase model. Note that agreement/disagreement between the measurement and predictions of Im(σ_{xy}) in Figs. 3(c) and 3(d) is over the entire measurement range (0–0.8 eV). In order to address the disagreement between Berry phase predictions and the data, we explore the low frequency intrinsic AHE response from quasiparticles in the calculation for AHE $\sigma_{xy}(E)$. The (d_{xz},d_{yz})-orbital tight-binding model considers contributions to the anomalous velocity from quasiparticle hopping between two d orbitals.[16,28,29] Ferromagnetic $\mathrm{Ca}_x\mathrm{Sr}_{1-x}\mathrm{RuO}_3$ is a good candidate for the (d_{xz},d_{yz})-orbital tight-binding model. Although $\mathrm{Ca}_x\mathrm{Sr}_{1-x}\mathrm{RuO}_3$ forms a large variety of compounds with different properties, the Fermi surface is mostly composed of Ru ions. Electrons in Sr and Ca ion do not appear at the Fermi level. The magnetic moment is provided by Ru 4d orbitals, which produce spin-orbit interactions with conduction electrons. Therefore, the quasiparticle hopping between d orbitals is critical to understanding optical conductivity in $\mathrm{Ca}_x\mathrm{Sr}_{1-x}\mathrm{RuO}_3$.

The interorbital quasiparticle hopping integral t' between next-nearest neighbors determines the overall behavior of $\sigma_{xy}(E)$ in the (d_{xz},d_{yz})-orbital tight-binding model.[29] For the calculation we use the interorbital nearest neighbor hopping integral $t = 200$ meV corresponding to the bandwidth of ruthenates and the spin-orbit interaction $\lambda = 30$ meV.[28] Additionally, the lattice constant $a = 4$ Å is used in all Ca compositions. In particular, the quasiparticle damping rate γ and minimum band splitting Δ are used as fitting parameters, which are a function of t', to investigate the measured conductivity of $Ca_xSr_{1-x}RuO_3$. Here, we do not consider the Ca doping dependence of Δ. The AHE $\sigma_{xy}(E)$ in Figs. 3(a) and 3(c) are well reproduced when $\Delta = 82$ meV ($t'/t = 0.05$) and $\gamma = 20$, 40, and 80 meV, which describe the AHE $\sigma_{xy}(E)$ for Ca compositions $x = 0$–0.13, 0.2, and 0.4, respectively. The damping rate γ due to elastic scattering is nearly proportional to x. Both the calculation and the measurement of the AHE Im(σ_{xy}) in Figs. 3(c) and 3(d) display clearly the dip and broadening near $E = \Delta$. In addition, both the calculations and measurements show significant changes in magnitude and shape along with the shift of the dip to higher energies as the Ca composition increases. For $x \geqslant 0.2$, the measured AHE Im(σ_{xy}) displays a small peak near $E = \Delta$, which is not seen in the calculation. The broadening of AHE Re(σ_{xy}) at $E = \Delta$ in Fig. 3(a) is given by γ. The fitted values of Δ and γ from $\sigma_{xy}(E)$ are applied to reproduce $\sigma_{xx}(E)$ in Figs. 2(a) and 2(c). The calculation is highly consistent with the measurement in magnitude and trend of $\sigma_{xx}(E)$ for all Ca compositions. The dc conductivity $\sigma_{xx}(0)$ is proportional to $1/\gamma$, and can be expressed as $\sigma_{xx}(0) = C/\gamma$, where $C = 325$ eV Ω^{-1} cm^{-1} is determined in the calculation. At energies below 0.3 eV, both the calculation and measurement show that $\sigma_{xx}(E)$ is sensitive to Ca composition. Although there are limited data points below 0.3 eV, the agreement/disagreement between the measurements and the theoretical predictions are clear, especially when one includes the dc data. Additionally, since the data points at 0.1 eV and 0.2 eV were taken by using bright laser light sources, these have significantly smaller error bars than data at higher energies, which were obtained using weaker broadband light sources. This clearly shows the dominance of the quasiparticle contribution over the Berry phase, especially at low energies. Note that all the given and the fitted parameters used in the tight-binding model are summarized in Table I.

Here, we discuss the intrinsic AHE $\sigma_{xy}(E)$ in more detail. An analytical expression for the AHE $\sigma_{xy}(E)$ is given as $\sigma_{xy}(E) = \sigma^{I}_{xy}(E) + \sigma^{II}_{xy}(E)$, where $\sigma^{I}_{xy}(E)$ is a Fermi surface term and $\sigma^{II}_{xy}(E)$ is a Fermi sea term contributed by quasiparticles with finite damping rate γ.[29] A part of the Fermi sea term includes the Berry curvature term.[2] Since the Berry curvature term cancels other contributions in the Fermi sea term, the entire Fermi sea term is weak typically and then the Fermi surface term dominates the AHE $\sigma_{xy}(E)$. According to the tight-binding model, if the calculation only considers the Berry curvature term, it is difficult to reproduce both the measured $\sigma_{xx}(E)$ and $\sigma_{xy}(E)$ because the estimated γ needs to be very large to fit the measured values. The (d_{xz},d_{yz})-orbital tight-binding model for the intrinsic term describes well both $\sigma_{xx}(E)$ and $\sigma_{xy}(E)$ over a wide energy range for the low Ca-doping case. However, the sign change in $\sigma_{xy}(E)$ at Ca composition $x = 0.4$ cannot be explained by this simple model. The disagreement with the measurement may be due to the changes in the local lattice structure of the system and their effect on the band structure. Alternately, the possible existence of a small Fermi pocket with small hybridization gap could cause this sign change.

Hall sign reversal with temperature for $SrRuO_3$ appears near the Curie temperature T_c where the remanent magnetization disappears for both dc and 117 meV measurements.[4,30] The sign reversal of dc $\rho_{xy}(T)$ is seen up to Ca composition $x = 0.3$. The dc Hall sign reversal temperature is severely reduced from the Curie temperature as Ca is added.[5] For $x = 0.13$, the dc Hall sign reversal occurs at $T = 60$ K, which is far from $T_c = 120$ K. There have been several theoretical attempts to explain the dc Hall sign reversal. Both the intrinsic Berry phase and extrinsic scattering mechanisms can explain the dc Hall sign reversal for $SrRuO_3$.[4] Furthermore, the Berry phase mechanism explains the dc Hall sign reversals of $\rho_{xy}(T)$ at the Ca composition from $x = 0$ to 0.4.[2,7] The temperature dependence of θ_F is measured for $x \leqslant 0.4$ at two midinfrared energies 117 meV and 224 meV, as shown in Figs. 4(a)–4(d). The midinfrared Hall sign reversal is observed only at 117 meV for the Ca composition from 0 to 0.13, which is a narrower range of x than for the dc Hall results. The infrared Hall sign reversal temperature is similar to that found at dc. The Hall sign reversal with T is clearly observable in the ferromagnetic hysteresis of the infrared AHE $\theta_F(H)$ as shown in Figs. 4(e) and 4(f). For $SrRuO_3$, it is difficult to recognize the Hall sign reversal near T_c due to the small hysteresis loop. For the Ca composition $x = 0.13$, it is easy to detect the inverted hysteresis loop because the Hall sign reversal temperature is well below $T_c = 120$ K. As shown in Figs. 4(a) and 4(c), the sign reversal temperature occurs at 60 K for the AHE Re(θ_F) and 50 K for the AHE Im(θ_F) at 117 meV. The AHE Re(θ_F) in Fig. 4(e) above and below $T = 60$ K displays the hysteresis loops that change from a step down to a step up near $H = 0$ T and the AHE Im(θ_F) in Fig. 4(f) above and below $T = 50$ K show similar behavior. At the higher energy of 224 meV, AHE θ_F in Figs. 4(b) and 4(d) changes monotonically with temperature without showing any Hall sign reversal.

TABLE I. (d_{xz},d_{yz})-orbital tight-binding model parameters.

Parameters		Description
Given[28]	$t = 200$ meV	Interorbital nearest neighbor hopping integral
	$\lambda = 30$ meV	Spin-orbit interaction
	$a = 4$ Å	Lattice constant
Fitted σ_{xy}	$\Delta(t/t' = 0.05) = 82$ meV	Minimum band splitting
	$\gamma = 20$ meV (for $x = 0$–0.13)	Quasiparticle damping rate
	$\gamma = 40$ meV (for $x = 0.2$)	
	$\gamma = 80$ meV (for $x = 0.4$)	
Fitted σ_{xx}	$C = 325$ eV Ω^{-1}cm^{-1}	dc $\sigma_{xx} = C/\gamma$

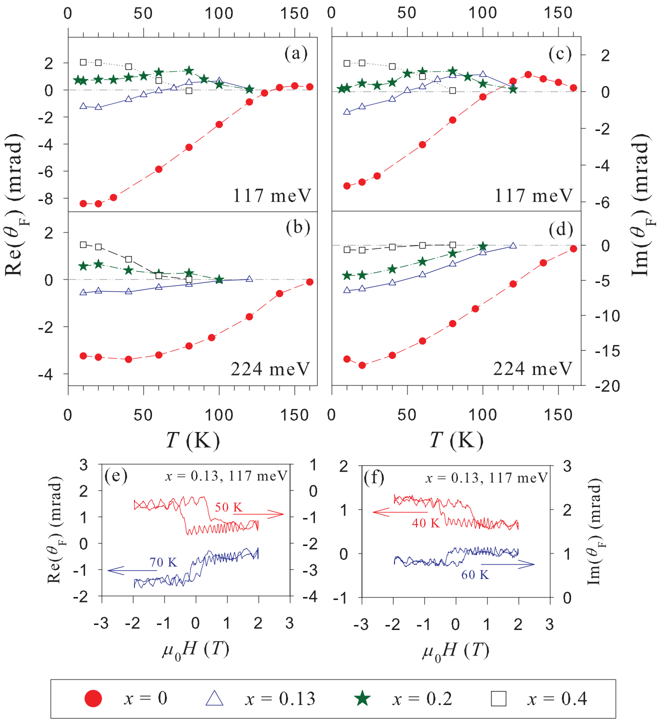

FIG. 4. (Color online) Temperature and magnetic field dependences of the infrared AHE θ_F for the Ca composition from $x = 0$ to 0.4. The temperature dependent AHE $\mathrm{Re}(\theta_F)$ at (a) 117 meV and (b) 224 meV. The temperature dependent AHE $\mathrm{Im}(\theta_F)$ at (c) 117 meV and (d) 224 meV. Both $\mathrm{Re}(\theta_F)$ and $\mathrm{Im}(\theta_F)$ were measured at $H = 0$ T with the sample fully magnetized out of plane in the temperature range from 10 K up to 160 K. The hysteresis loops of (e) $\mathrm{Re}(\theta_F)$ at two temperatures 50 K and 70 K and (f) $\mathrm{Im}(\theta_F)$ at two temperatures 40 K and 60 K were observed for the Ca composition $x = 0.13$. The sign change of the hysteresis loops appears near $H = 0$ T. Note that the error bar is about 10–20% above 40 K and a few percent below 20 K.

Probing the AHE as a function of temperature, Ca doping, and frequency is critical to understanding the rich AHE, including sign reversals, in this family of materials. By adding another new dimension, frequency, to the AHE experiments, we have greatly extended the parameter space that theories can explore and have placed new constraints on these theories. Future theoretical work will have to take into account our dc and infrared Hall sign reversal data when explaining the mechanisms behind the AHE. For example, if the Hall sign reversal is due to the quasiparticle contribution, the infrared Hall angle should be a function of the quasiparticle scattering rate and will be zero when the scattering rate reaches a specific value. If the Hall sign reversal vs temperature occurs above the quasiparticle scattering energy, the sign reversal mechanism is probably due to the intrinsic Berry phase contribution.

IV. PARAMAGNETIC REGION ($x \geqslant 0.75$)

The symmetric nature of the Hall angle around QPT is of particular interest in the paramagnetic state of $\mathrm{Ca}_x\mathrm{Sr}_{1-x}\mathrm{RuO}_3$ films. dc Hall resistivity measurements exhibit symmetric behavior with x near QPT,[5] but this has not been explored yet at midinfrared energies due to the following two challenges. First of all, the infrared Hall angle in the paramagnetic state is typically much smaller than in the ferromagnetic state. Secondly, it is experimentally challenging to separate the AHE from the overall Hall angle because the paramagnetic response is almost linear with the applied magnetic field just like the OHE response. We present here θ_F and θ_K from the paramagnetic $\mathrm{Ca}_x\mathrm{Sr}_{1-x}\mathrm{RuO}_3$ in the energy range from 0.1 eV to 0.7 eV and at various temperatures. Our experimental sensitivity is 10^{-4} rad, which can clearly resolve the paramagnetic signal at $H = 1$ T. Since the OHE contribution is expected to be smaller at higher probing energy,[4] we are assuming that the MNIR θ_F and θ_K are dominated by the AHE.

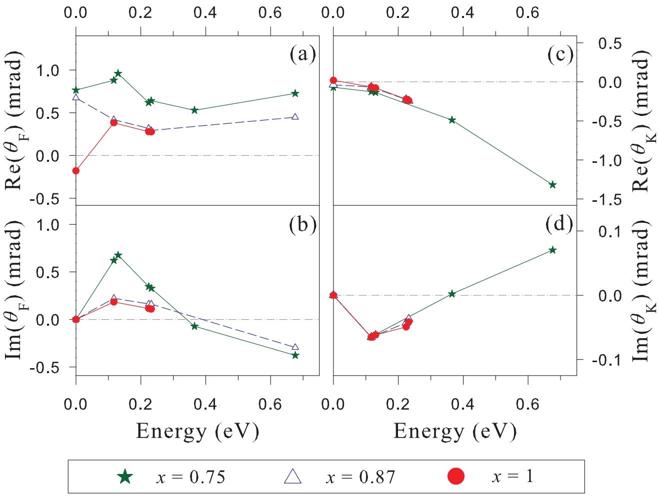

FIG. 5. (Color online) Energy dependence of θ_F and θ_K for the Ca composition $x = 0.75$–1. (a) $\mathrm{Re}(\theta_F)$, (b) $\mathrm{Im}(\theta_F)$, (c) $\mathrm{Re}(\theta_K)$, and (d) $\mathrm{Im}(\theta_K)$ at $H = 1$ T and $T = 10$ K. θ_F and θ_K include contributions from the ordinary Hall effect. The dc values of $\mathrm{Re}(\theta_F)$ and $\mathrm{Re}(\theta_K)$ in (a) and (c) are determined in Ref. 5.

The negative sign of the dc Hall angle in CaRuO_3 at low temperature and its sign reversal at higher temperature are remarkable since they more closely resemble the behavior in ferromagnetic SrRuO_3 (Ref. 5) than CaRuO_3's paramagnetic neighbors, which have a strictly positive dc Hall angle. The negative Hall angle at dc can be reversed by adding very small concentrations of Sr. Figure 5 shows the energy dependent θ_F and θ_K at $H = 1$ T and $T = 10$ K for Ca composition from $x = 0.75$ to 1. The $\mathrm{Re}(\theta_F)$ in Fig. 5(a) for CaRuO_3 is negative at dc, but becomes positive at finite energies. All other paramagnetic compounds have a positive dc $\mathrm{Re}(\theta_F)$. Peaks of $\mathrm{Re}(\theta_F)$ and $\mathrm{Im}(\theta_F)$ at 0.1 eV can be found at both $x = 0.75$ and $x = 0.47$. In addition, both infrared $\mathrm{Im}(\theta_F)$ cross zero near 0.3 eV. A dip in $\mathrm{Im}(\theta_K)$ at 0.1 eV is seen at both concentrations. The similarities of θ_F and θ_K for the $x = 0.75$ of the paramagnetic compound in Fig. 5 and the $x = 0.47$ of the ferromagnetic compound in Fig. 1 confirm the symmetric nature of the Hall angle around QPT. θ_K exhibits a much weaker dependence on Ca concentration than θ_F. Figure 6 shows θ_F at 117 meV and $H = 1$ T for Ca composition ranging from 0.75 to 1 as a function of temperature. No Hall sign reversal is observed, unlike the reversal seen in the dc ρ_{xy} for CaRuO_3.[5] All paramagnetic compounds have

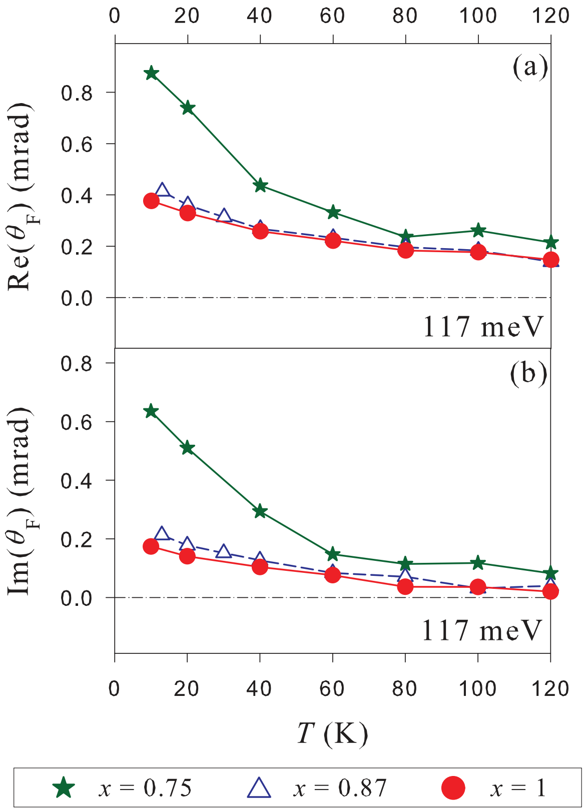

FIG. 6. (Color online) Temperature dependence of the infrared θ_F for the Ca composition $x = 0.75$–1. (a) Re(θ_F) and (b) Im(θ_F) at 117 meV and $H = 1$ T. θ_F includes the OHE contribution.

the same temperature dependence of θ_F, which approaches zero as temperature rises. The energy and temperature dependence θ_F for CaRuO$_3$ in Figs. 5 and 6 indicates that the negative dc Hall angle of CaRuO$_3$ is very sensitive to both probing energy and the Sr substitution. Moreover, the origin for the strikingly similar behavior of the dc θ_H at opposite ends of the Ca$_x$Sr$_{1-x}$RuO$_3$ composition range remains unknown.

V. CONCLUSION

We compare predictions from the (d_{xz},d_{yz})-orbital tight-binding model, which accounts for the quasiparticle contribution to the intrinsic AHE, to infrared AHE measurements. The model reproduces well the low energy response of both $\sigma_{xx}(E)$ and $\sigma_{xy}(E)$ for ferromagnetic Ca$_x$Sr$_{1-x}$RuO$_3$. More accurate predictions would require a LDA band calculation constructing a realistic multiorbital tight-binding model for Ca$_x$Sr$_{1-x}$RuO$_3$. The infrared Hall angle reverses sign with temperature for Ca$_x$Sr$_{1-x}$RuO$_3$ only for $x = 0$ and 0.13 at 117 meV. The Hall sign reversal temperatures at dc and at 117 meV are the same in these two compounds. The origins of the infrared Hall sign reversals with temperature remain unknown. According to Refs. 16, 28, and 29, the sign change of $\sigma_{xy}(T)$ can be understood by taking the temperature dependence of the quasiparticle damping rate γ into account. We also have examined the infrared Hall response in paramagnetic Ca$_x$Sr$_{1-x}$RuO$_3$. The Hall effect mechanism for paramagnetic Ca$_x$Sr$_{1-x}$RuO$_3$ is still unknown, but infrared Hall data provide insight for new developing theories on these paramagnetic materials such as the intrinsic anomalous Hall response due to the paramagnetic band structure or the extrinsic response due to the quasiparticle scattering in the paramagnetic materials.[1]

ACKNOWLEDGMENTS

The authors thank H. D. Drew for helpful discussions. We also wish to thank P. Khalifah for providing us the dc data and Z. Fang for the calculation data of Berry phase contribution. This work was supported by the Research Corporation for Science Advancement Cottrell Scholar Grant, the National Science Foundation (NSF) NSF-CAREER-DMR0449899, and NSF-DMR1006078.

---

[1] N. Nagaosa, J. Sinova, S. Onoda, A. H. MacDonald, and N. P. Ong, Rev. Mod. Phys. **82**, 1539 (2010).

[2] Z. Fang, N. Nagaosa, K. S. Takahashi, A. Asamitsu, R. Mathieu, T. Ogasawara, H. Yamada, M. Kawasaki, Y. Tokura, and K. Terakura, Science **302**, 92 (2003).

[3] Y. Kats, I. Genish, L. Klein, J. W. Reiner, and M. R. Beasley, Phys. Rev. B **70**, 180407(R) (2004).

[4] M.-H. Kim, G. Acbas, M.-H. Yang, M. Eginligil, P. Khalifah, I. Ohkubo, H. Christen, D. Mandrus, Z. Fang, and J. Cerne, Phys. Rev. B **81**, 235218 (2010).

[5] P. Khalifah, I. Ohkubo, B. C. Sales, H. M. Christen, D. Mandrus, and J. Cerne, Phys. Rev. B **76**, 054404 (2007).

[6] S. C. Gausepohl, M. Lee, R. A. Rao, and C. B. Eom, Phys. Rev. B **54**, 8996 (1996).

[7] R. Mathieu, A. Asamitsu, H. Yamada, K. S. Takahashi, M. Kawasaki, Z. Fang, N. Nagaosa, and Y. Tokura, Phys. Rev. Lett. **93**, 016602 (2004).

[8] R. Mathieu, C. U. Jung, H. Yamada, A. Asamitsu, M. Kawasaki, and Y. Tokura, Phys. Rev. B **72**, 064436 (2005).

[9] J. Smit, Physica **21**, 877 (1955).

[10] J. Smit, Physica **24**, 39 (1958).

[11] J. Smit, Phys. Rev. B **8**, 2349 (1973).

[12] W.-L. Lee, S. Watauchi, V. L. Miller, R. J. Cava, and N. P. Ong, Science **303**, 1647 (2004).

[13] T. Jungwirth, Q. Niu, and A. H. MacDonald, Phys. Rev. Lett. **88**, 207208 (2002).

[14] R. Karplus and J. M. Luttinger, Phys. Rev. **95**, 1154 (1954).

[15] L. Berger, Phys. Rev. B **2**, 4559 (1970).

[16] H. Kontani, T. Tanaka, and K. Yamada, Phys. Rev. B **75**, 184416 (2007).

[17] G. Acbas, M.-H. Kim, M. Cukr, V. Novák, M. A. Scarpulla, O. D. Dubon, T. Jungwirth, J. Sinova, and J. Cerne, Phys. Rev. Lett. **103**, 137201 (2009).

[18] J. M. Harris, Y. F. Yan, and N. P. Ong, Phys. Rev. B **46**, 14293 (1992).

[19] J. Cerne, M. Grayson, D. C. Schmadel, G. S. Jenkins, H. D. Drew, R. Hughes, A. Dabkowski, J. S. Preston, and P.-J. Kung, Phys. Rev. Lett. **84**, 3418 (2000).

[20] A. Zimmers, L. Shi, D. C. Schmadel, W. M. Fisher, R. L. Greene, H. D. Drew, M. Houseknecht, G. Acbas, M.-H. Kim, M.-H. Yang, J. Cerne, J. Lin, and A. Millis, Phys. Rev. B **76**, 064515 (2007).

[21] J. Sinova, T. Jungwirth, J. Kučera, and A. H. MacDonald, Phys. Rev. B **67**, 235203 (2003).

[22] H. D. Drew and P. Coleman, Phys. Rev. Lett. **78**, 1572 (1997).

[23] J. Cerne, D. C. Schmadel, L. B. Rigal, and H. D. Drew, Rev. Sci. Instrum. **74**, 4755 (2003).

[24] M.-H. Kim, G. Acbas, M.-H. Yang, I. Ohkubo, H. Christen, D. Mandrus, M. A. Scarpulla, O. D. Dubon, Z. Schlesinger, P. Khalifah, and J. Cerne, Phys. Rev. B **75**, 214416 (2007).

[25] M.-H. Kim, V. Kurz, G. Acbas, C. T. Ellis, and J. Cerne, J. Opt. Soc. Am. B **28**, 199 (2011).

[26] P. Khalifah, I. Ohkubo, H. M. Christen, and D. G. Mandrus, Phys. Rev. B **70**, 134426 (2004).

[27] I. Ohkubo, H. M. Christen, P. Khalifah, S. Sathyamurthy, H. Y. Zhai, C. M. Rouleau, D. G. Mandrus, and D. H. Lowndes, Appl. Surf. Sci. **223**, 35 (2004).

[28] H. Kontani, T. Tanaka, D. S. Hirashima, K. Yamada, and J. Inoue, Phys. Rev. Lett. **100**, 096601 (2008).

[29] T. Tanaka and H. Kontani, Phys. Rev. B **77**, 195129 (2008).

[30] R. Shimano, Y. Ikebe, K. S. Takahashi, M. Kawasaki, N. Nagaosa, and Y. Tokura, Europhys. Lett. **95**, 17002 (2011).